Drug-Dependent Morphological Transitions in Spherical and Worm-Like Polymeric Micelles Define Stability and Pharmacological Performance of Micellar Drugs

Chaemin Lim, Jacob D. Ramsey, Duhyeong Hwang, Susana C. M. Teixeira, Chi-Duen Poon, Joshua D. Strauss, Elias P. Rosen, Marina Sokolsky-Papkov, and Alexander V. Kabanov*

<u>SUPPLEMENT</u>

Drug-dependent morphological transitions in spherical and worm-like micelles define stability and pharmacological performance of micellar drugs

Dr. Chaemin Lim [1], Jacob D. Ramsey [1], Dr. Duhyeong Hwang [1], Dr. Susana C. M. Teixeira [2, 3], Dr. Chi-Duen Poon [4], Prof. Joshua D Strauss [5], Prof. Elias P. Rosen [6], Prof. Marina Sokolsky-Papkov [1], Prof. Alexander V. Kabanov [1, 7, *]

[1] Center for Nanotechnology in Drug Delivery and Division of Pharmacoengineering and Molecular Pharmaceutics, Eshelman School of Pharmacy, University of North Carolina at Chapel Hill, NC 27599, USA

[2] Department of Chemical and Biomolecular Engineering, University of Delaware, 150 Academy Street, Newark, DE 19716, USA

[3] NIST Center for Neutron Research, National Institute of Standards and Technology, 100 Bureau Drive, Gaithersburg, MD 20899, USA

[4] Research Computer Center University of North Carolina Chapel Hill, NC 27599, USA

[5] Department of Biochemistry and Biophysics, School of Medicine, University of North Carolina at Chapel Hill, Chapel Hill, NC, USA.

[6] Eshelman School of Pharmacy, University of North Carolina at Chapel Hill, NC 27599, USA

[7] Laboratory of Chemical Design of Bionanomaterials, Faculty of Chemistry, M.V. Lomonosov Moscow State University, Moscow 119992, Russia

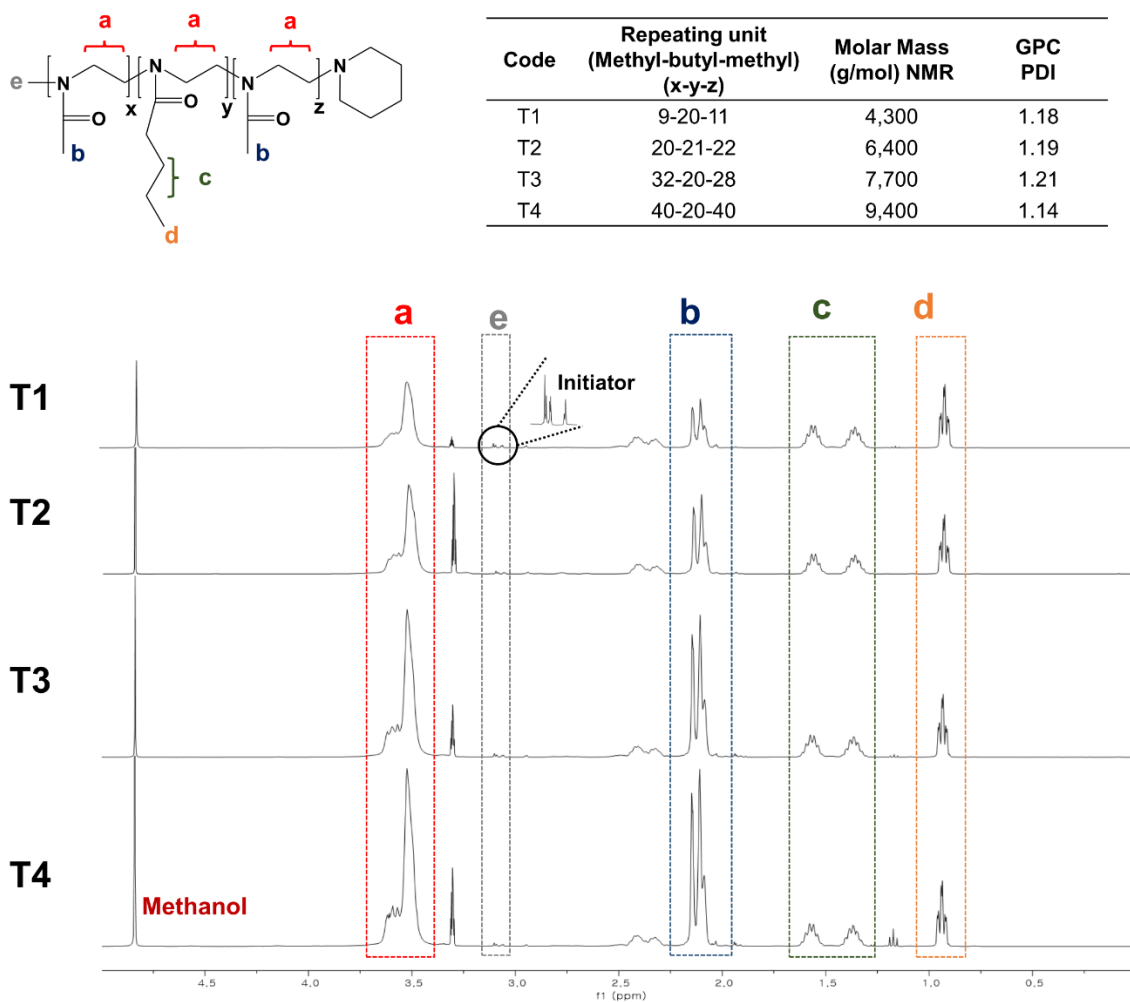* Corresponding author's email: kabanov@email.unc.edu

Code	Repeating unit (Methyl-butyl-methyl) (x-y-z)	Molar Mass (g/mol) NMR	GPC PDI
T1	9-20-11	4,300	1.18
T2	20-21-22	6,400	1.19
T3	32-20-28	7,700	1.21
T4	40-20-40	9,400	1.14

Figure S1. Structure, NMR spectra, and molecular characteristics of the poly(2-oxazoline)-based triblock copolymers used in this study. (GPC PDI, polydispersity index based on Gel Permeation Chromatography (GPC), see **Figure S2**).
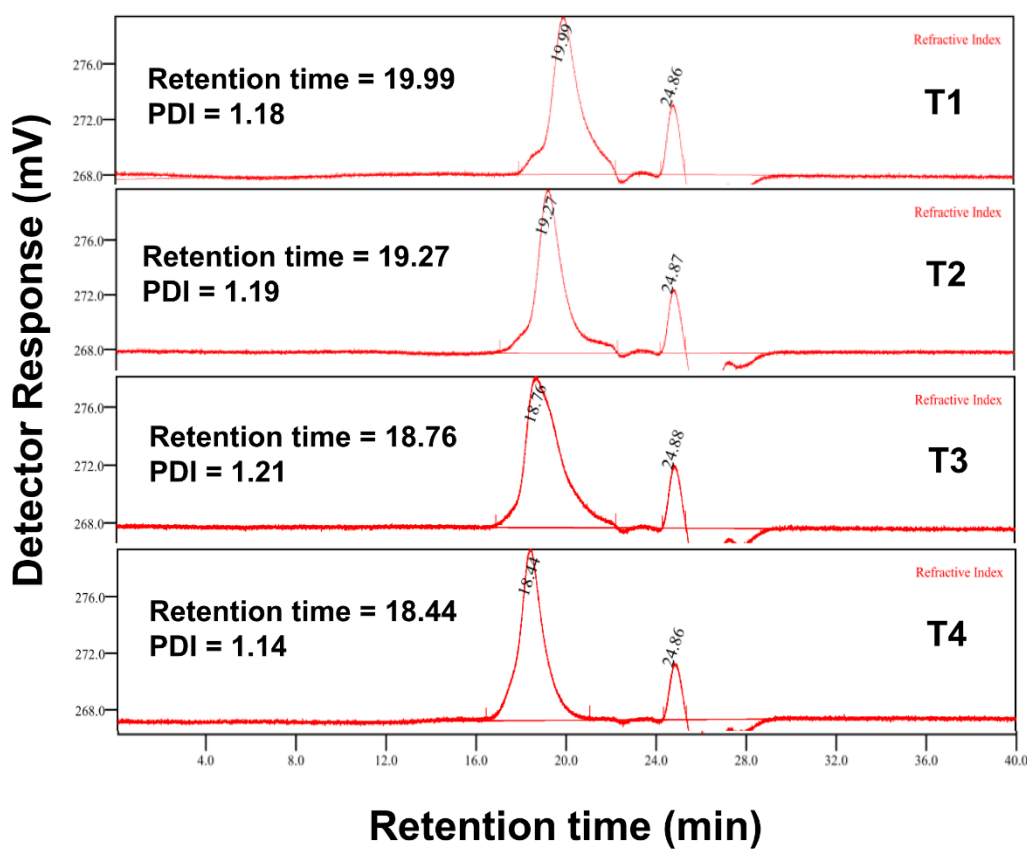
Figure S2. To determine the value of polymer PDI, molecular mass distribution of the copolymers was analyzed by GPC on a GPC-max VE2001 system (RI detector mode, PSS SEC column (GRAM 100 Å 8 × 300 mm, SDV 5 μm) with N,N-dimethylformamide (DMF) (25 mM LiBr, 1 mL/min) as eluent and calibrated against polymethylmethacrylate standards. The GPC PDI values suggested narrow molecular mass distribution of the polymers.

(a)
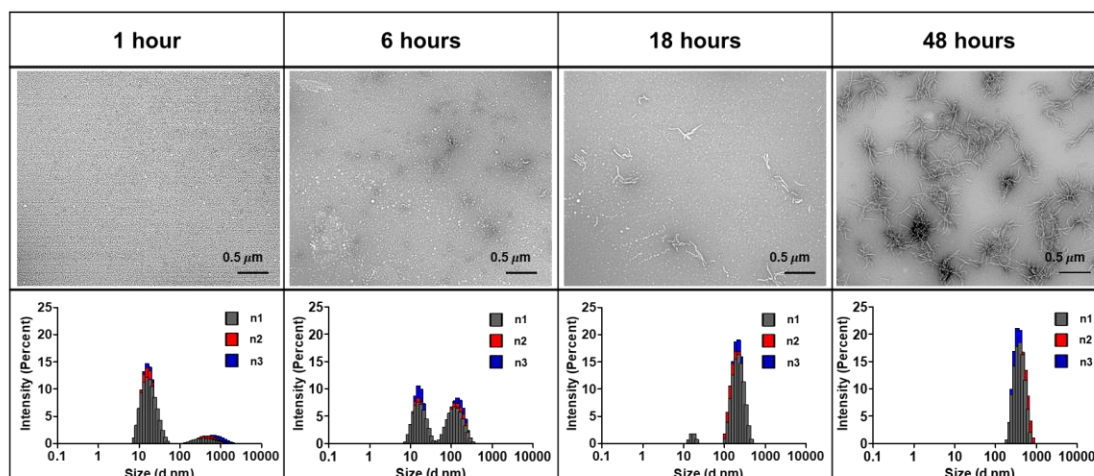
(b)

Polymer Conc. (mg/mL)	1 hour		6 hours		24 hours		48 hours	
	Size (nm)	PDI	Size (nm)	PDI	Size (nm)	PDI	Size (nm)	PDI
1.25	39.2 ± 1.8	0.62 ± 0.15	64.9 ± 1.0	0.51 ± 0.02	148.7 ± 3.9	0.15 ± 0.02	186.3 ± 4.5	0.16 ± 0.02
2.5	31.2 ± 9.2	0.38 ± 0.10	52.4 ± 1.0	0.55 ± 0.01	158.4 ± 2.6	0.18 ± 0.03	212.3 ± 1.6	0.15 ± 0.03
5	20.2 ± 0.2	0.32 ± 0.02	40.4 ± 0.9	0.54 ± 0.02	169.7 ± 3.3	0.20 ± 0.02	263.7 ± 7.5	0.17 ± 0.03
10	18.1 ± 0.1	0.27 ± 0.01	30.9 ± 0.5	0.54 ± 0.01	185.9 ± 19.3	0.23 ± 0.04	346.7 ± 5.1	0.14 ± 0.05
20	17.3 ± 0.1	0.26 ± 0.01	26.0 ± 0.6	0.47 ± 0.01	179.4 ± 7.9	0.32 ± 0.01	449 ± 21.4	0.22 ± 0.02
40	17.4 ± 0.6	0.31 ± 0.03	27.1 ± 0.9	0.54 ± 0.07	227.9 ± 5.1	0.34 ± 0.02	775.9 ± 22.5	0.27 ± 0.07
80	20.0 ± 0.6	0.53 ± 0.01	28.7 ± 1.0	0.78 ± 0.02	331.8 ± 7.4	0.32 ± 0.01	1857 ± 127.7	0.36 ± 0.01

Temp.	1 hour		6 hours		24 hours		48 hours	
	Size (nm)	PDI	Size (nm)	PDI	Size (nm)	PDI	Size (nm)	PDI
4 °C	18.4 ± 1.3	0.27 ± 0.09	32.0 ± 1.7	0.46 ± 0.03	118.4 ± 5.2	0.21 ± 0.01	146.6 ± 14.7	0.17 ± 0.02
25 °C	18.1 ± 0.1	0.27 ± 0.01	30.9 ± 0.5	0.54 ± 0.01	185.9 ± 19.3	0.23 ± 0.04	346.7 ± 5.1	0.14 ± 0.05
40 °C	24.1 ± 1.1	0.42 ± 0.02	65.0 ± 2.8	0.60 ± 0.03	233.8 ± 24.3	0.28 ± 0.03	342.0 ± 35.3	0.26 ± 0.08

Salt conc.	1 hour		6 hours		24 hours		48 hours	
	Size (nm)	PDI	Size (nm)	PDI	Size (nm)	PDI	Size (nm)	PDI
0%	20.2 ± 0.2	0.32 ± 0.02	40.4 ± 0.9	0.54 ± 0.02	169.7 ± 3.3	0.20 ± 0.02	263.7 ± 7.5	0.17 ± 0.03
0.5%	18.5 ± 1.3	0.13 ± 0.08	27.0 ± 3.7	0.37 ± 0.05	127.1 ± 9.0	0.48 ± 0.10	254.8 ± 8.9	0.26 ± 0.03
1%	20.3 ± 0.9	0.21 ± 0.02	24.7 ± 1.5	0.36 ± 0.02	110.9 ± 7.5	0.61 ± 0.03	245.6 ± 7.6	0.26 ± 0.03
2%	21.1 ± 0.9	0.21 ± 0.01	24.1 ± 1.5	0.33 ± 0.03	88.7 ± 1.9	0.60 ± 0.04	209.1 ± 7.6	0.28 ± 0.04
4%	26.0 ± 1.0	0.29 ± 0.04	27.7 ± 0.7	0.38 ± 0.05	69.6 ± 10.8	0.61 ± 0.03	165.7 ± 7.1	0.36 ± 0.03

Figure S3. (a) Evolution of the particle morphology and intensity weighted size distribution of the T2 polymeric micelles in distilled water (10 mg/mL, 25ºC), visualized by TEM. **(b)** Particle size and PDI of the T2 polymeric micelles under various conditions, to examine: the effect of polymer concentration (in distilled water and at 25℃), temperature (10 mg/mL polymer concentration in distilled water) and ionic strength (5 mg/mL polymer concentration at 25℃). Elongation was favored by increasing the concentration and temperature and inhibited by increasing the ionic strength. The errors shown correspond to three standard deviation of uncertainty.

Table S1. Loading parameters (LC, LE)[a], DLS (Dynamic light scattering) particle size (D_z), and polydispersity (PDI) of the micelles at different drug loadings (polymer/drug w/w ratios of 10/1, 10/2, 10/4 and 10/8). The errors shown represent three standard deviation of uncertainty.

	Drug	LC_{max} (%)	LE_{max} (%)	10/1		10/2		10/4		10/8	
				Size (nm)	PDI	Size (nm)	PDI	Size (nm)	PDI	Size (nm)	PDI
T2	Bortezomib	43.4 ± 1.3	97.5 ± 3.0	16.2 ± 1.2	0.16 ± 0.06	15.8 ± 0.2	0.15 ± 0.02	16.3 ± 0.3	0.08 ± 0.02	22.6 ± 1.8	0.10 ± 0.06
	Olaparib	27.3 ± 1.0	93.9 ± 4.8	14.7 ± 1.0	0.13 ± 0.05	18.3 ± 1.5	0.19 ± 0.06	20.5 ± 3.3	0.13 ± 0.01	N/A	
	Etoposide	42.0 ± 2.9	91.0 ± 10.6	15.5 ± 0.5	0.08 ± 0.02	18.2 ± 2.0	0.14 ± 0.02	18.2 ± 1.9	0.17 ± 0.04	25.3 ± 4.6	0.09 ± 0.02
	Resiquimod	43.4 ± 1.0	95.7 ± 3.8	21.4 ± 4.3	0.19 ± 0.02	20.5 ± 3.9	0.19 ± 0.01	17.6 ± 0.8	0.19 ± 0.04	19.9 ± 1.2	0.25 ± 0.03
	BLZ945	42.5 ± 1.9	92.7 ± 7.5	23.7 ± 2.0	0.28 ± 0.03	20.7 ± 1.9	0.15 ± 0.05	20.3 ± 0.9	0.12 ± 0.03	27.5 ± 2.6	0.03 ± 0.01
	Rapamycin	26.5 ± 0.8	90.1 ± 3.8	22.8 ± 2.6	0.22 ± 0.06	19.8 ± 1.0	0.19 ± 0.03	22.0 ± 1.4	0.04 ± 0.03	N/A	
	RXDX-105	27.6 ± 1.9	95.5 ± 8.8	24.3 ± 2.5	0.15 ± 0.04	20.3 ± 1.8	0.19 ± 0.11	24.1 ± 3.2	0.19 ± 0.12	N/A	
	AZD2014	28.4 ± 1.1	99.4 ± 5.5	31.1 ± 2.7	0.15 ± 0.08	20.1 ± 0.5	0.25 ± 0.03	19.2 ± 0.3	0.11 ± 0.04	N/A	
	AZD8055	44.3 ± 1.0	99.3 ± 4.0	20.4 ± 3.0	0.25 ± 0.08	19.1 ± 0.2	0.16 ± 0.01	21.8 ± 0.6	0.11 ± 0.03	28.8 ± 0.5	0.03 ± 0.02
	Selumetinib	17.0 ± 0.2	102.1 ± 1.3	14.9 ± 1.0	0.14 ± 0.07	20.2 ± 6.0	0.19 ± 0.06	N/A		N/A	
	PLX3397	27.8 ± 1.5	96.7 ± 7.3	18.6 ± 0.5	0.21 ± 0.03	22.5 ± 1.5	0.25 ± 0.08	54.9 ± 0.8	0.17 ± 0.03	N/A	
	ABT-263	27.8 ± 0.7	96.3 ± 3.4	20.2 ± 4.7	0.17 ± 0.03	20.8 ± 2.5	0.16 ± 0.06	24.9 ± 0.8	0.19 ± 0.03	N/A	
	Vismodegib	27.3 ± 1.7	94.0 ± 8.0	18.1 ± 0.8	0.06 ± 0.01	19.1 ± 1.3	0.05 ± 0.02	24.8 ± 2.1	0.08 ± 0.01	N/A	
	Paclitaxel	27.1 ± 2.4	92.9 ± 11.2	16.2 ± 0.6	0.03 ± 0.01	18.6 ± 0.9	0.07 ± 0.01	18.0 ± 0.5	0.12 ± 0.01	N/A	
T3	Bortezomib	43.5 ± 1.2	97.9 ± 2.7	18.5 ± 2.2	0.15 ± 0.01	17.7 ± 2.8	0.12 ± 0.01	19.9 ± 2.9	0.12 ± 0.01	107.6 ± 8.3	0.06 ± 0.04
	Olaparib	28.1 ± 0.9	97.5 ± 4.5	18.0 ± 3.0	0.11 ± 0.05	17.4 ± 0.6	0.14 ± 0.02	20.2 ± 2.7	0.16 ± 0.03	N/A	
	Etoposide	43.2 ± 0.5	95.0 ± 1.9	17.5 ± 1.2	0.09 ± 0.02	18.2 ± 2.1	0.10 ± 0.04	20.3 ± 2.1	0.08 ± 0.02	33.1 ± 1.6	0.13 ± 0.01
	Resiquimod	42.3 ± 2.9	91.9 ± 11.2	22.1 ± 6.3	0.10 ± 0.03	19.9 ± 3.3	0.20 ± 0.01	21.3 ± 2.8	0.23 ± 0.01	26.4 ± 2.7	0.21 ± 0.03
	BLZ945	42.8 ± 1.9	93.7 ± 7.2	19.3 ± 0.4	0.09 ± 0.04	23.7 ± 3.0	0.13 ± 0.07	40.2 ± 6.5	0.16 ± 0.03	87.9 ± 1.4	0.09 ± 0.03
	Rapamycin	42.6 ± 2.2	92.8 ± 8.1	19.9 ± 1.0	0.10 ± 0.02	20.8 ± 0.7	0.07 ± 0.05	29.2 ± 1.5	0.08 ± 0.05	53.5 ± 3.4	0.19 ± 0.06
	RXDX-105	42.5 ± 2.1	92.8 ± 7.9	33.5 ± 1.0	0.18 ± 0.02	36.6 ± 0.5	0.17 ± 0.05	32.8 ± 0.4	0.13 ± 0.02	81.4 ± 7.2	0.22 ± 0.02
	AZD2014	27.8 ± 1.3	96.3 ± 6.3	19.2 ± 0.5	0.13 ± 0.04	19.5 ± 0.3	0.13 ± 0.02	22.3 ± 1.9	0.13 ± 0.06	N/A	
	AZD8055	43.3 ± 2.1	95.7 ± 7.9	24.4 ± 3.2	0.22 ± 0.03	23.1 ± 0.7	0.17 ± 0.06	34.6 ± 0.4	0.25 ± 0.02	77.2 ± 15.9	0.23 ± 0.02
	Selumetinib	28.3 ± 1.3	95.6 ± 6.4	17.2 ± 0.1	0.10 ± 0.02	25.2 ± 8.0	0.20 ± 0.06	30.3 ± 3.1	0.16 ± 0.03	N/A	
	PLX3397	43.8 ± 1.5	97.4 ± 6.2	26.9 ± 0.3	0.20 ± 0.01	23.6 ± 0.8	0.11 ± 0.02	31.1 ± 1.3	0.14 ± 0.04	88.7 ± 1.1	0.19 ± 0.03
	ABT-263	42.5 ± 1.2	92.4 ± 4.7	25.8 ± 2.1	0.25 ± 0.01	40.0 ± 1.1	0.23 ± 0.03	54.4 ± 1.0	0.13 ± 0.01	82.0 ± 2.1	0.05 ± 0.03
	Vismodegib	42.8 ± 1.7	93.7 ± 6.7	20.6 ± 0.5	0.11 ± 0.01	21.1 ± 2.5	0.08 ± 0.04	27.1 ± 3.9	0.04 ± 0.05	41.4 ± 4.3	0.11 ± 0.03
	Paclitaxel	43.0 ± 1.3	94.4 ± 4.9	20.8 ± 1.4	0.11 ± 0.02	24.0 ± 0.3	0.09 ± 0.04	33.6 ± 0.9	0.20 ± 0.02	54.1 ± 5.9	0.15 ± 0.05

[a] Loading capacity, $LC\,\% = \dfrac{mass\ drug\ loaded}{mass\ drug\ loaded + mass\ polymer\ used} \times 100$; Loading efficiency, $LE\,\% = \dfrac{mass\ drug\ loaded}{mass\ drug\ added} \times 100$

PLX3397 even at low loadings formed unstable micelle formulations, which precipitated without apparent formation of worms after 24 hours. In other cases, precipitation was observed only after high drug loadings.
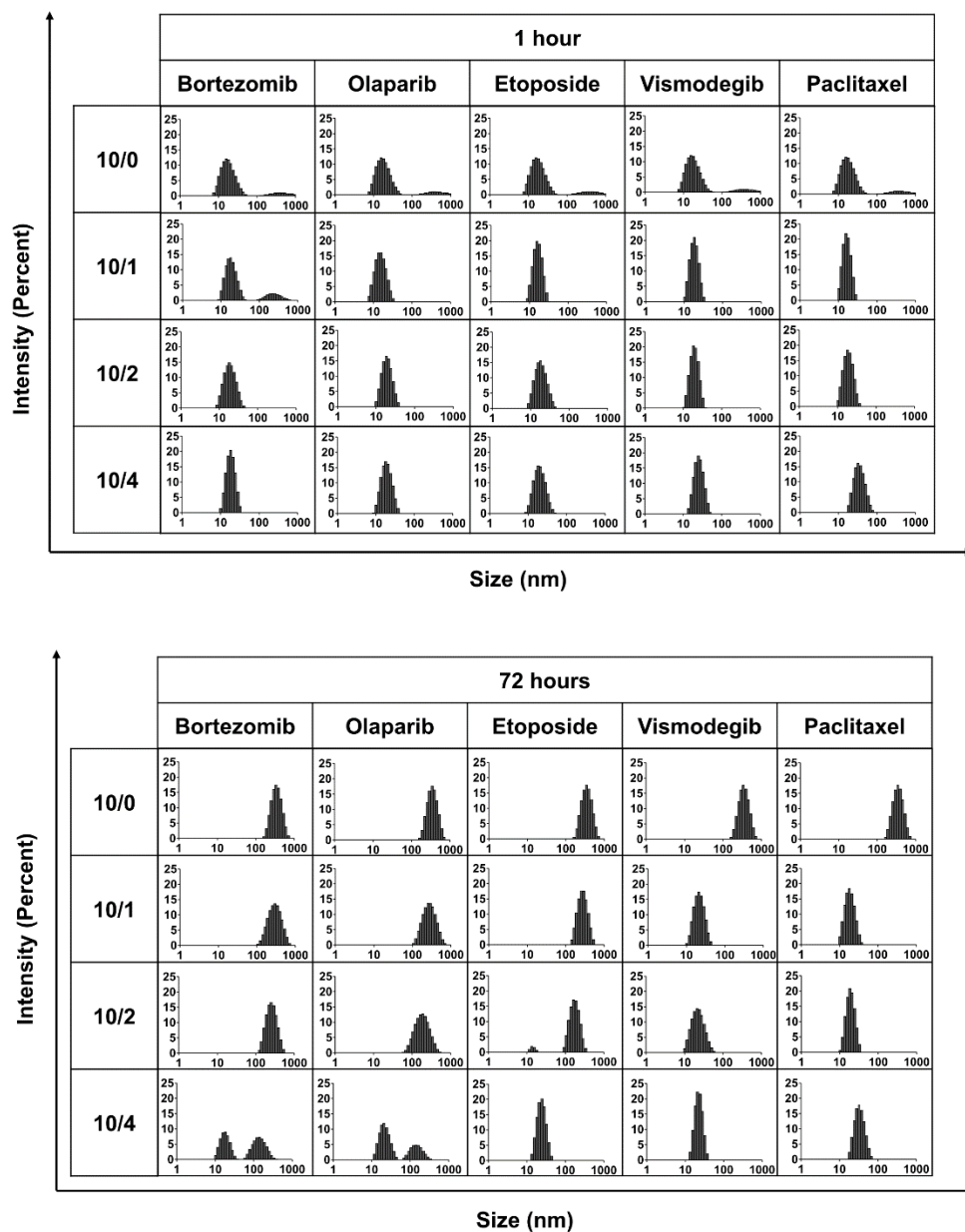
Figure S4. Change in size distribution of T2-based polymeric micelles at various drug loading ratios over time (polymer/drug ratios of 10/1, 10/2, and 10/4). Representative data for aggregation of T2. Small spherical micelles, with the particle size of ca. 20–30 nm, are observed at short incubation times, both in the drug-free micelle solutions and/or in the presence of worm-inhibiting drugs at high drug loadings. The observed increase over time in particle size, up to several hundred nm, is indicative of worm formation. The intensity weighted distributions are shown.
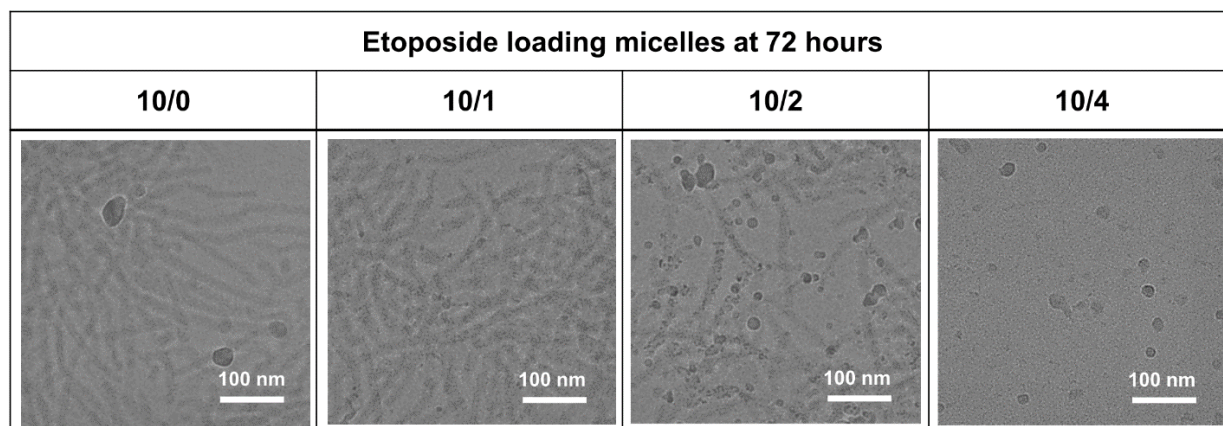
Etoposide loading micelles at 72 hours			
10/0	**10/1**	**10/2**	**10/4**

Figure S5. Cryo-TEM images of T2 aggregates in the presence and absence of various amounts of etoposide at room temperature, after 72 hours. T2 concentration 10 mg/mL in saline (0.9 % NaCl).

	Drug	1 hour					24 hours					48 hours					72 hours				
		10/0	10/1	10/2	10/4	10/8	10/0	10/1	10/2	10/4	10/8	10/0	10/1	10/2	10/4	10/8	10/0	10/1	10/2	10/4	10/8
25°C	Bortezomib	S	S	S	S	S	W+S	W+S	S	S	S	W+S	W+S	S	S	S	W+S	W+S	W+S	S	S
	Olaparib	S	S	S	S	P	W+S	S	S	S	P	W+S	W+S	S	S	P	W+S	W+S	W+S	S	P
	Resiquimod	S	S	S	S	S	W+S	S	S	S	P	W+S	W+S	S	P	P	W+S	W+S	P	P	P
	Etoposide	S	S	S	S	S	W+S	S	S	S	S	W+S	S	S	S	S	W+S	W+S	W+S	S	S
	BLZ945	S	S	S	S	S	W+S	S	S	S	P	W+S	S	P	P	P	W+S	P	P	P	P
	Rapamycin	S	S	S	S	S	W+S	S	S	S	S	W+S	S	S	S	S	W+S	S	S	S	S
	RXDX-105	S	S	S	S	S	W+S	S	S	S	P	W+S	S	S	S	P	W+S	S	S	S	P
	AZD2014	S	S	S	S	P	W+S	S	S	S	P	W+S	S	S	S	P	W+S	S	S	S	P
	AZD8055	S	S	S	S	S	W+S	S	S	S	S	W+S	S	S	S	P	W+S	S	S	S	P
	Selumetinib	S	S	S	S	P	W+S	S	S	S	P	W+S	S	S	S	P	W+S	S	S	S	P
	PLX3397	S	S	S	S	S	W+S	P	P	P	P	W+S	P	P	P	P	W+S	P	P	P	P
	ABT-263	S	S	S	S	S	W+S	S	S	S	S	W+S	S	S	S	S	W+S	S	S	S	S
	Vismodegib	S	S	S	S	S	W+S	S	S	S	S	W+S	S	S	S	S	W+S	S	S	S	S
	Paclitaxel	S	S	S	S	S	W+S	S	S	S	S	W+S	S	S	S	S	W+S	S	S	S	S
4°C	Bortezomib	S	S	S	S	S	S	S	S	S	S	S	S	S	S	S	S	S	S	S	S
	Olaparib	S	S	S	S	P	S	S	S	S	P	S	S	S	S	P	S	S	S	S	P
	Resiquimod	S	S	S	S	S	S	S	S	S	P	S	S	S	P	P	S	S	S	P	P
	Etoposide	S	S	S	S	S	S	S	S	S	S	S	S	S	S	S	S	S	S	S	S
	BLZ945	S	S	S	S	S	S	S	S	S	S	S	S	S	S	P	S	S	S	P	P
	Rapamycin	S	S	S	S	S	S	S	S	S	S	S	S	S	S	S	S	S	S	S	S
	RXDX-105	S	S	S	S	S	S	S	S	S	P	S	S	S	S	P	S	S	S	S	P
	AZD2014	S	S	S	S	P	S	S	S	S	P	S	S	S	S	P	S	S	S	S	P
	AZD8055	S	S	S	S	S	S	S	S	S	S	S	S	S	S	P	S	S	S	S	P
	Selumetinib	S	S	S	S	P	S	S	S	S	P	S	S	S	S	P	S	S	S	S	P
	PLX3397	S	S	S	S	S	S	P	P	P	P	S	P	P	P	P	S	P	P	P	P
	ABT-263	S	S	S	S	S	S	S	S	S	S	S	S	S	S	S	S	S	S	S	S
	Vismodegib	S	S	S	S	S	S	S	S	S	S	S	S	S	S	S	S	S	S	S	S
	Paclitaxel	S	S	S	S	S	S	S	S	S	S	S	S	S	S	S	S	S	S	S	S

Figure S6. Monitoring the sphere-to-worm transition process of T3-based polymeric micelles at various drug loadings ratio over time (polymer/drug w/w ratios of 10/1, 10/2, 10/4 and 10/8). Although some T3 micelles also show the sphere-to-worm transition, this transition is predominantly absent in this sample set.

SANS data on T2 micelle systems

Attempts were made to fit the blank micelle SANS data using a uniform scattering length density cylindrical model. However, the results showed poor agreement with the data at higher scattering angles (not shown). Calculated contour length and cylinder radius were also inconsistent with the light scattering and cryo-TEM results. A core-shell cylindrical model provided poor agreement with the scattering profiles for both blank and lower drug concentration solutions, where a worm-like micelle structure was plausible. Instead, small angle neutron scattering data were fitted using the following functional form:

$$I(q) = \frac{A}{q^n} + I_{micelle} + B,$$

where the first term describes Porod scattering from clusters of spherical micelles, B is the incoherent background and $I_{micelle}$ describes scattering from individual T2 spherical micelles (blank or drug loaded) and q is the momentum transfer, defined as:

$$q = \frac{4\pi}{\lambda} \sin\theta$$

The micelles were modelled as core-shell spherical particles with constant ratio between the core radius and the total radius. Micelle interactions were modelled as hard-sphere interactions. The fitting parameters are shown in **Table S2**. The reduced Chi-squared values are defined as:

$$Reduced\ Chi^2 = \sqrt{\chi^2/(N - f - 1)},$$

where N is the number of data points used in the fit, and f is the number of degrees of freedom. For the lower scattering angle data, with large size aggregates and micelles clusters with dimensions outside the resolution of the collected data, the polydispersity significantly reduces the quality of the fits. For higher concentrations of paclitaxel and etoposide, the fitting range was limited to the higher q-range, where the main scattering contributions are due to the single micelles in solution.

Table S2. Fitting parameters of SANS data corresponding to the T2 solution at various drug loading ratios (polymer/drug weight ratios of 10/1, 10/2, and 10/4). Errors shown correspond to one standard deviation of uncertainty. Parameters without reported errors were kept fixed during the fitting of the SANS data.

(a)

Fit parameters		Olaparib			Etoposide		
	10/0	10/1	10/2	10/4	10/1	10/2	10/4
Coefficient A (x10^{-6})	8	20	28	34	29	35	40
Power (n)	3	2.88	2.82	2.1	2.7	2.55	2.0
Volume fraction	0.009	0.011	0.012	0.014	0.011	0.012	0.014
Core radius (Å)	41.3 ± 0.8	43.2 ± 0.6	45.2 ± 0.5	47.8 ± 0.1	43.0 ± 0.8	43.7 ± 0.1	48.7 ± 0.1
Overall polydispersity	0.36	0.36	0.34	0.20	0.40	0.25	0.20
SLD Core (x10^{-6} Å^{-2})	1.2 ± 0.1	0.7 ± 0.1	1.0 ± 0.1	0.4 ± 0.1	1.1 ± 0.1	0.9 ± 0.3	1.1 ± 0.3
Shell Thickness (Å)	29.7 ± 0.7	28.8 ± 0.3	28.8 ± 0.3	23.2 ± 0.4	26.1 ± 0.7	25.2 ± 0.1	25.4 ± 0.1
SLD Shell (x10^{-6} Å^{-2})	4.1 ± 0.1	4.5 ± 0.1	4.7 ± 0.1	6.1 ± 0.1	5.1 ± 0.1	5.4 ± 0.1	5.9 ± 0.2
SLD solvent (x10^{-6} Å^{-2})	6.4	6.4	6.4	6.4	6.4	6.4	6.4
Background (x10^{-3} cm^{-1})	1.8	0.8	1.0	1.5	2.0	0.3	0.2
Reduced Chi^2	3.3	2.9	4.5	4.2	2.5	5.4	4.1

(b)

Fit parameters		Paclitaxel			Vismodegib		
	10/0	10/1	10/2	10/4	10/1	10/2	10/4
Coefficient A (x10^{-6})	8	210	400	800	250	550	600
Power (n)	3	2	1	1	1.6	1.6	1
Volume fraction	0.009	0.011	0.012	0.014	0.011	0.012	0.014
Core radius (Å)	41.3 ± 0.8	41.0 ± 0.1	47.6 ± 0.1	55.0 ± 0.1	46.6 ± 0.1	49.3 ± 0.1	61.4 ± 0.1
Overall polydispersity	0.36	0.20	0.16	0.15	0.14	0.18	0.13
SLD Core (x10^{-6} Å^{-2})	1.2 ± 0.1	0.7 ± 0.1	0.7 ± 0.1	0.7 ± 0.1	0.8 ± 0.1	0.1 ± 0.1	0.5 ± 0.3
Shell Thickness (Å)	29.7 ± 0.7	22.0 ± 0.2	21.8 ± 0.2	21.7 ± 0.2	23.5 ± 0.3	23.8 ± 0.1	27.0 ± 0.1
SLD Shell (x10^{-6} Å^{-2})	4.1 ± 0.1	5.2 ± 0.1	5.6 ± 0.1	5.4 ± 0.1	5.7 ± 0.1	5.6 ± 0.1	5.7 ± 0.1
SLD solvent (x10^{-6} Å^{-2})	6.4	6.4	6.4	6.4	6.4	6.4	6.4
Background (x10^{-3} cm^{-1})	1.8	0.0	0.1	0.0	0.1	0.5	0.1
Reduced Chi^2	3.3	210	400	800	250	550	600

Measuring effective value of critical micelle concentration (CMC) by DLS count rate of polymeric micelles

Previous work indicates that drugs in POx micelle could have specific interaction with the backbone structure of the poly(2-oxazoline) and with components of the hydrophilic shell-forming block, dependent on loading amount [1]. These interactions could offer additional stability to the spherical morphology and could lower the CMC and chemical potential inhibiting the transition to worm-like structure both in terms of its thermodynamic favorability and the kinetics due to an increase of the potential barriers between morphological forms. We use here effective CMC* terminology to acknowledge that in some cases the formed aggregates (e.g., spherical micelles in the absence of any drug) are metastable and transform to worm-like micelles over time. However, since the transition is very slow (days) as a first approximation an equilibrium between the micellar aggregates and single block copolymer chains can be characterized by effective CMC*. As pointed out before the effective CMC* can be considered as a surrogate metric of the thermodynamic stability of polymeric micelles [2]. One additional consideration of the effective CMC* in this study is that the drug loaded micelles undergo partitioning of the solubilized drug into aqueous phase upon dilution [3]. This can complicate the interpretation of the CMC* value especially at high drug loadings since the drug loaded micelles are *de facto* a multicomponent system comprising both the drug and the block copolymer components. We have selected DLS as the method for estimating the effective CMC* values as point of deflection (e.g., slope change) in the intensity of light scattering indicating disassembly of the block copolymer or block copolymer and drug aggregates. There is an inherent limitation of this method in comparing CMC* for different morphologies, because the DLS intensity signal is more sensitive to the particles of larger size, e.g., worm-like vs. spherical. With this consideration in mind, we characterized the changes in the CMC* and used this as a metric for micelle stability at various drug loadings within the same morphology. Overall, as drug loading increased, the CMC* value gradually decreased indicating an increase in stability against dilution - likely the result of increased drug-polymer intermolecular interactions in the micelle. While all the drugs studied displayed the same trend, they did so with different magnitudes. For instance, vismodegib and paclitaxel, which belong to the micelle elongation-inhibiting group, produce greater shifts in the CMC* when encapsulated into spherical micelles suggesting greater micelle stabilization than etoposide or olaparib. It is clear that the lower CMC* of the drug-loaded spherical micelles (estimated as 82.2 μg/mL and 53.3 μg/mL for vismodegib and paclitaxel and 198.3 μg/mL and 175 μg/mL for etoposide and olaparib at a 10/4 polymer/drug w/w ratio) indicate an increased stability of such micelles and explain why the elongation behavior was different across the different drugs.
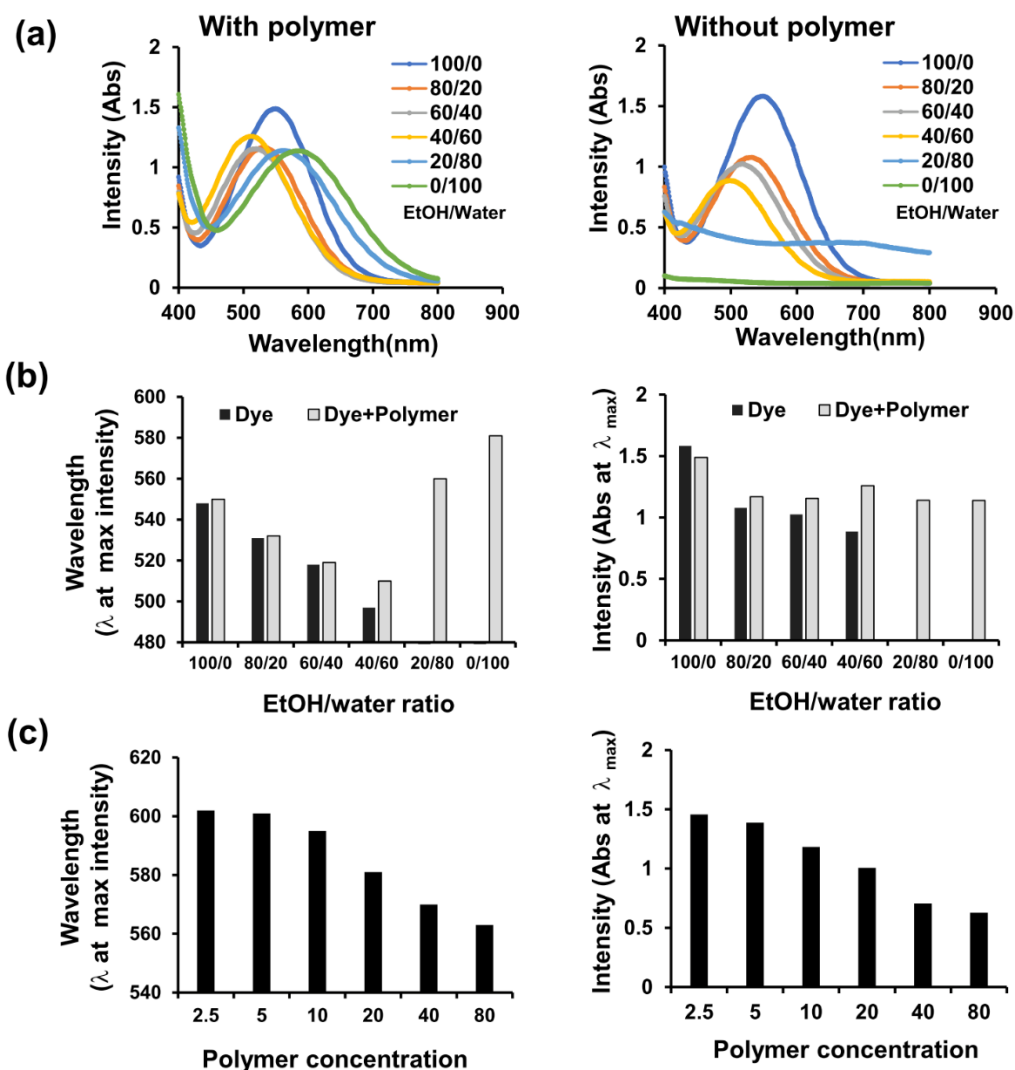
Figure S7. (a) Derived count rate of polymeric micelles with gradual dilution of samples at various drug loading ratios (polymer/drug w/w ratios of 10/0, 10/1, 10/2, and 10/4). **(b)** Derived count rate (kilo-counts per second (kcps)) plot with enlarged Y-axis used to measure the effective CMC*; the point of slope change in the derived count rate was defined as the CMC*. A T2 concentration of 1 mg/mL was used in distilled water at 25°C.

Figure S8. (a) UV-Vis absorption spectra of Reichardt's dye (RD) at various ethanol/water solvent volume ratios (100/0, 80/20, 60/40, 40/60, 20/80, and 0/100), with and without T2 (10 mg/mL). **(b, c)** Wavelength at the maximal absorbance (λ_{max}) and maximal absorbance (Abs) of RD in **(b)** ethanol/water mixtures (corresponding to spectra in plots **(a)**) and in **(c)** aqueous solutions at various polymer concentrations. RD (0.5 mg/mL, 25 °C) was diluted either in **(a, b)** distilled water or **(c)** saline (0.9 % NaCl). The λ_{max} of RD decreases as the polarity of the microenvironment increases; from a λ_{max} of 548 nm in ethanol (100 %) to a λ_{max} of 497 nm in the ethanol/water mixture (40 % / 60 %). The λ_{max} of the RD in the POx micelles was higher compared to both the pure ethanol and the ethanol-water mixture, at any polymer concentration above the CMC. This is due to the relative hydrophobic environment maintained by 2-butyl-2-oxazoline core. However, as the polymer concentration increased, λ_{max} decreased, suggesting transfer of the dye within the micelles in polar environments. This was accompanied by a decrease in the dye absorbance, indicating specific interactions between the dye and the polymer.
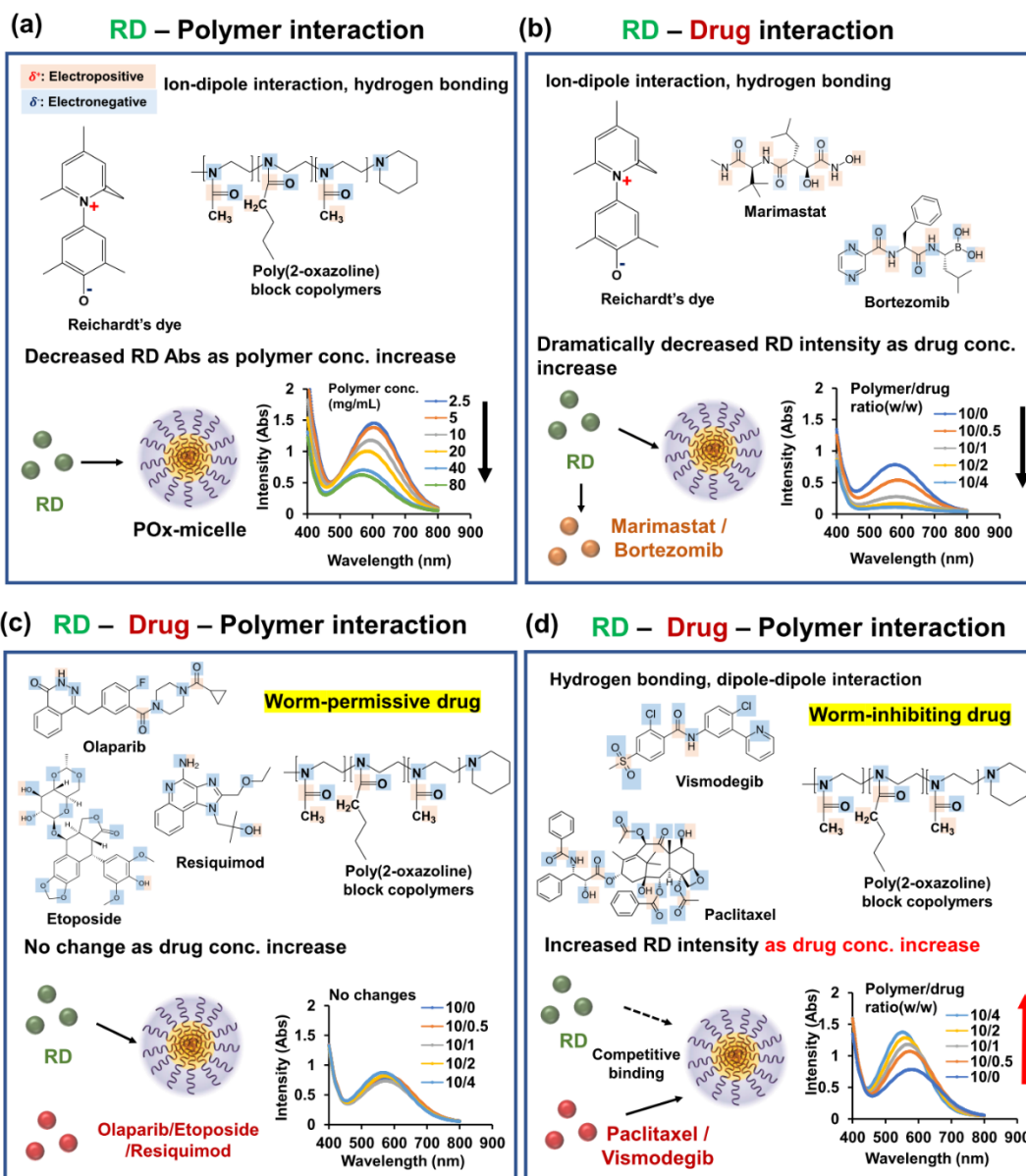
Figure S9. Schematic representation of the RD, polymer, and drug interactions resulting in the observed changes in dye absorbance intensity. **(a)** The betaine RD molecule may interact with the repeating amide bond motifs in the POx block copolymer resulting in attenuation of the dye absorbance. **(b)** Co-loading of the RD in the micelles with marimastat and bortezomib having a repeating amide bond motif results in further attenuation of the dye absorbance intensity. **(c)** The drugs without the amide bond motifs do not interact with the RD and therefore do not change its absorbance intensity. **(d)** Worm-inhibiting drugs such as paclitaxel and vismodegib interact strongly with the same binding sites in the polymer and displace the RD, increasing the dye absorbance intensity.
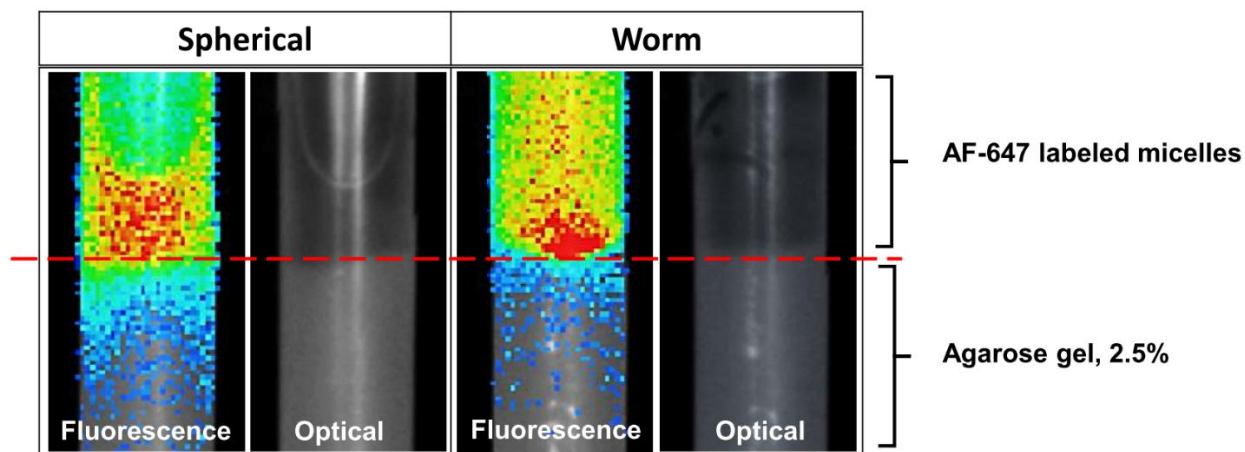
Figure S10. Simulation of drug-loaded micelle penetration. Dye-labeled spherical or worm-structured micelles (10/1 polymer/drug ratio, 10 mg/mL of T2 in 0.9 % NaCl) were added into a column containing 2.5 % agarose gel and incubated for 24 hours under a water flow. The red dashed line indicates the border line between the water and agarose gel. Spherical micelles showed better penetration in the model.

Table S3. Particle size and PDI of olaparib-loaded micelles (polymer/drug ratio of 10/1) over time in the presence of BSA. Polymer concentrations are 10 mg/mL in each condition.

Spherical micelles

BSA Conc. (mg/mL)	1 hour		6 hours		24 hours		48 hours		72 hours	
	Size (nm)	PDI	Size (nm)	PDI	Size (nm)	PDI	Size (nm)	PDI	Size (nm)	PDI
0	14.7±1.0	0.13±0.05	37.6±17.6	0.37±0.14	128.9±4.1	0.26±0.06	230.9±18	0.19±0.01	309.2±52.6	0.15±0.06
5	13.4±0.4	0.16±0.03	13.5±0.2	0.16±0.02	38.7±1.9	0.61±0.01	156.2±3.0	0.31±0.01	211.3±5.8	0.26±0.02
10	12.1±0.2	0.15±0.02	13.2±0.3	0.22±0.03	37.3±2.1	0.64±0.12	164.3±2.9	0.32±0.02	219.2±6.5	0.26±0.02
20	10.6±0.1	0.15±0.01	11.3±0.2	0.21±0.02	33.6±2.9	0.75±0.12	173.7±4.9	0.37±0.05	236.4±3.3	0.30±0.01

Worm-like-micelles (72 hours after initial preparation)

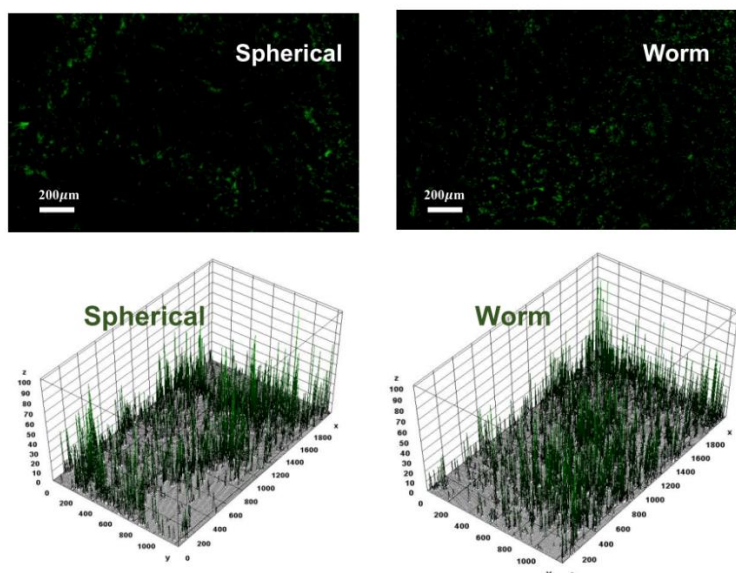| BSA Conc. (mg/mL)	1 hour		24 hours		48 hours	
	Size (nm)	PDI	Size (nm)	PDI	Size (nm)	PDI
5	331.8±3.5	0.20±0.01	374.6±14.5	0.20±0.01	400.4±2.6	0.22±0.04
10	343.8±8.1	0.19±0.03	365.9±1.8	0.22±0.03	408.8±7.6	0.23±0.01
20	350.4±14.3	0.24±0.02	377.4±7.2	0.23±0.03	391.9±12.4	0.26±0.05

Figure S11. Blood vessels were stained with an antibody against CD31. CD31 fluorescence intensity at tumor sections was visualized using 3D surface plots (Image J). X and Y axes represent the area of the tumor sections, and the Z axis represents the CD31 (Green) intensities. Polymer distributions in the same tissue sections and respective 3D surface plots are shown in **Figure 9c**.
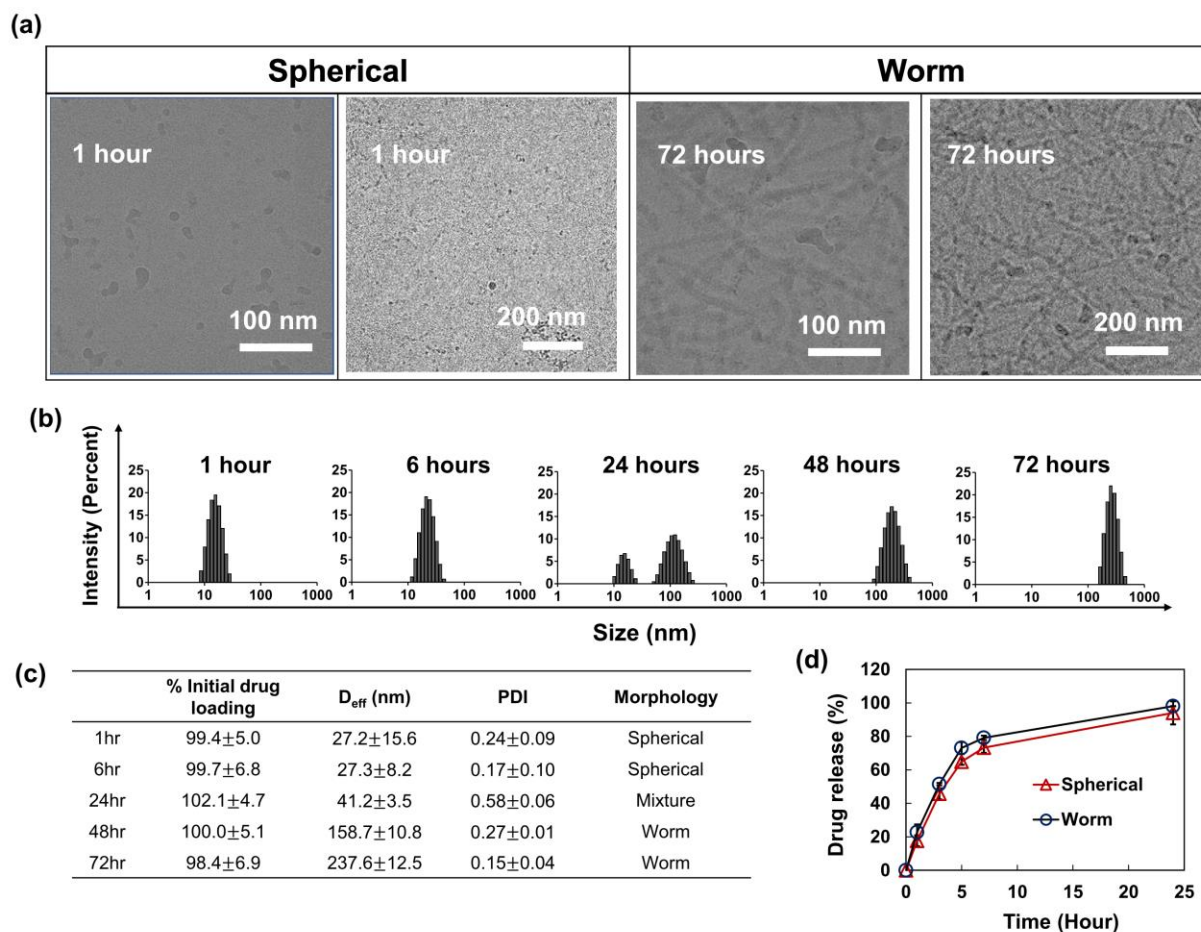
Figure S12. Preparation and characterization of selumetinib-loaded micelles (polymer/drug ratio of 10/0.5) with different morphologies. **(a)** Cryo-TEM images of selumetinib-loaded micelles at 1 hour and 72 hours after hydration. Change of **(b)** intensity weighted size distribution and **(c)** particle size, PDI, and drug concentration of selumetinib-loaded micelles over time. **(d)** Selumetinib release profile from sphere- and worm-like micelles. Selumetinib-loaded micelles were prepared using the thin film hydration method. While keeping drug loading content, the selumetinib micelles elongated until forming worm-like structure by 72 hours. Selumetinib micelles did not exhibit significant changes in the drug release profile. Errors shown correspond to three standard deviations of uncertainty.
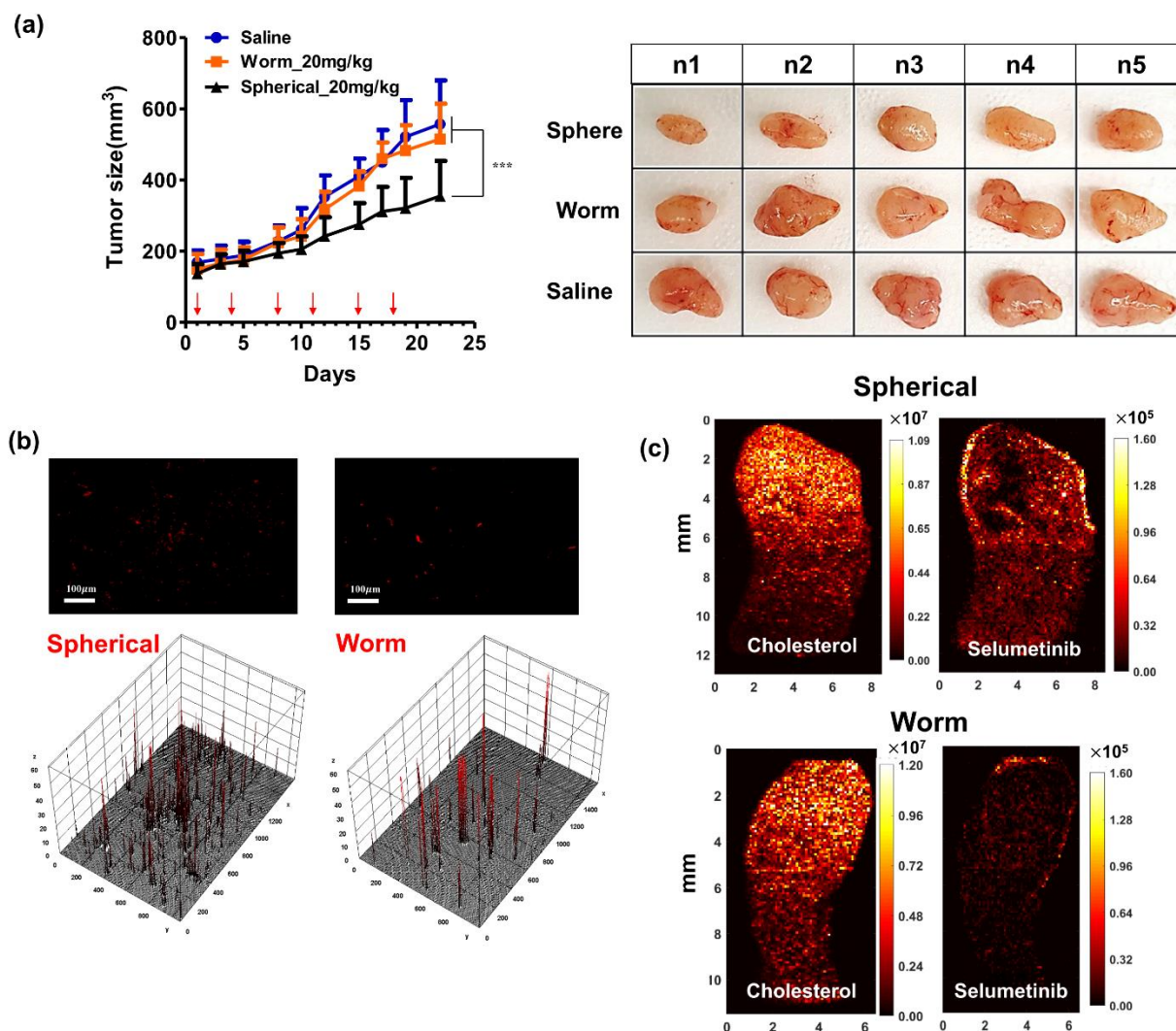
Figure S13. Antitumor activity and biodistribution of selumetinib loaded micelles (polymer/drug ratio of 10/0.5) in a tumor model (pancreatic carcinoma xenograft BXPC-3). **(a)** Tumor growth inhibition after 6 injections of selumetinib-loaded micelles (20 mg/kg), delivered twice a week (shown by arrows) (n=5). **(b)** Visualization and 3D surface plots (analyzed in Image J) of the distribution AF-647 labeled micelles in tumor sections 1 hour after injection **(c)** IR-MALDESI MSI analysis of selumetinib in tumor sections from mice following a single dose of selumetinib loaded micelles (20 mg/kg) at 1 hour. Statistical difference *** $p < 0.001$ for drug in spherical micelles vs. drug in worm-like micelles and saline control.

Table S4. AUC and clearance of polymer and drug in tumor and plasma after a single injection of olaparib (10 mg/kg) in the spherical (S) and worm-like (W) micelles (10/1 composition).

Location	PK Parameter [a]		Polymer			Drug		
			S	W	p[b]	S	W	p[b]
Tumor	AUC	Very early (0-1 h)	45.1	29	-	2.9	1.7	-
		Early (0-2 h)	95.5	66.2	-	4.6	2.9	-
		Late (2-24 h)	1371	1573	-	9.3	8.5	-
		Very late (8-24 h)	1016	1230	-	5.7	5.3	-
		AUC$_{all}$	1466	1639	ns	13.8	11.4	*
Plasma	AUC	Very early (0-1 h)	1146	1248	-	3.3	3.8	-
		Early (0-2 h)	1830	2175	-	5	5.8	-
		Late (2-24 h)	6169	7622	-	9.7	8.8	-
		Very late (8-24 h)	3314	4035	-	5	3.7	-
		AUC$_{all}$	8000	9796	*	14.7	14.6	ns
	CL (mL/h)		0.39	0.29	*	17.9	12.0	ns
	CL2 (mL/h)		1.92	0.53	ns	34.8	24.0	ns

[a] AUC$_{all}$ – Area under the curve from the time of dosing to the time of the last observation; CL-clearance blood; CL2 blood to organ intercompartmental clearance for the two-compartment model shown in **Figure S13**; [b] Significance S vs. W groups: *$p < 0.05$.

To obtain an in-depth view of the PK and tumor distribution of the drug and the polymer, we analyzed four different AUC periods in addition to the AUC$_{all}$ (**Table S4**): "very early" (0-1 hour), "early" (0-2 hour), "late" (2-24 hour), and very late (8-24 hour). Based on this analysis, we concluded that the drug and the polymer in the spherical micelles exhibited higher tumor AUC compared to the worm-like micelles during the early periods. The worm-like micelles also exhibited significantly decreased blood clearance (Cl) compared to the spherical micelles, as well as decreased intercompartmental clearance (Cl2) for both the polymer and the drug.
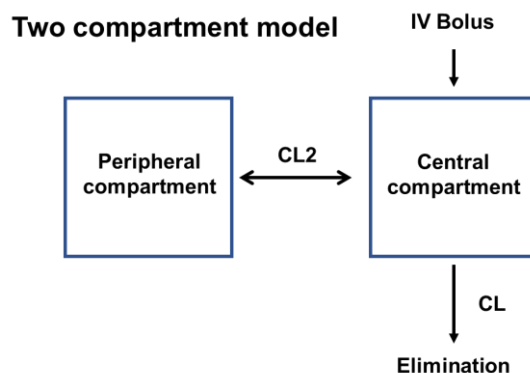
Two compartment model

Figure S14 Two-compartment model describing the delivery of the polymeric micelles to a tumor. The drug is administered as a bolus in the form of spherical or worm-like micelles and is subsequently distributed between the central compartment (plasma) and peripheral compartment (including tumor). The two-compartment model with IV-bolus dosing was the best fit for polymer and drug in both morphologies. Notably, the olaparib intercompartmental clearance (Cl2) was higher for the spherical micelles than the worm-like micelles, though not with statistical significance. This indicates that the drug in the spherical micelles is able to travel faster to tissues throughout the body (e.g., tumor), accumulating faster. The same phenomenon is seen for the polymer in spherical micelles. The intercompartmental transfer in these micelles is 4 times higher than that in the worm-like micelles. The rapid transfer of both the drug and polymer in the spherical micelles (i.e., to additional tissues) suggests that they can also rapidly accumulate in other tissues.

Disclaimer

Certain commercial equipment, instruments, suppliers are identified to foster understanding. This does not imply recommendation or endorsement by the National Institute of Standards and Technology, nor does it imply that the materials or equipment identified are necessarily the best available for the purpose.

References

[1]   A.-C. Pöppler, M. M. Lübtow, J. Schlauersbach, J. Wiest, L. Meinel, R. Luxenhofer, Angewandte Chemie International Edition 2019, 58, 18540.
[2]   A. V. Kabanov, I. R. Nazarova, I. V. Astafieva, E. V. Batrakova, V. Y. Alakhov, A. A. Yaroslavov, V. A. Kabanov, Macromolecules 1995, 28, 2303.
[3]   M. Y. Kozlov, N. S. Melik-Nubarov, E. V. Batrakova, A. V. Kabanov, Macromolecules 2000, 33, 3305.